Diapycnal Mixing I: Turbulence

Motivation: The thermohaline circulation has long been regarded as a consequence of diapycnal mixing.
Since the ocean is heated and cooled almost entirely at its surface, interior vertical mixing is necessary to maintain the thermohaline circulation. That is, mixing must warm the cold deep water to allow it to rise and make room for more cold water sinking at high latitudes. If there were no mixing, the deep water would stay uniformly cold and no additional water could sink. In fact, the mixing can be thought of as the driver for the thermohaline "conveyor belt", and it is clearly not a "heat engine" like the atmosphere.

Assuming:

(i) Incompressibility:

$$\frac{\partial u}{\partial x}+\frac{\partial v}{\partial y}+\frac{\partial w}{\partial z}=0$$

(ii) Thermal Wind:

$$\frac{\partial \mathbf{u}}{\partial z}=-\frac{g}{\rho_0 f}\mathbf{k}\times\nabla\rho$$

(iii) Vertical advective-diffusive balance (Munk, 1966):

$$w\frac{\partial \rho}{\partial z}=K\frac{\partial^2 \rho}{\partial z^2}$$

We obtain the scaling relationships:

$$UD = WL$$

$$\frac{\Delta\rho}{\rho_0} = \frac{fUL}{gD}$$

$$D = \frac{K}{W}$$

where *U,W* are the horizontal and vertical velocity scales, *L,D* are the horizontal and vertical length scales, and $\Delta\rho$ the north-south density difference at the surface.

This gives a thermocline thickness scale in terms of the density difference:

$$D = \left[\frac{fL^2 K}{g\Delta\rho / \rho_0} \right]^{1/3}$$

The strength of the meridional overturning is:

$$M = UDL = WL^2 = \left[\frac{g \Delta \rho L^4 K^2}{\rho_0 f} \right]^{1/3}$$

The poleward heat transport is:

$$Q = C \, \rho_0 c_p M \Delta T \approx K^{2/3}$$

where C is a constant (~0.25), c_p is the heat capacity, and ΔT is the north-south temperature difference.

Zhang, Schmitt and Huang (1999) have confirmed these scalings in a basin GCM, and examined the interplay with the additional density forcing due to the hydrologic cycle. For any given *K* a critical value of fresh water forcing is required to allow multiple solutions for the thermohaline circulation.

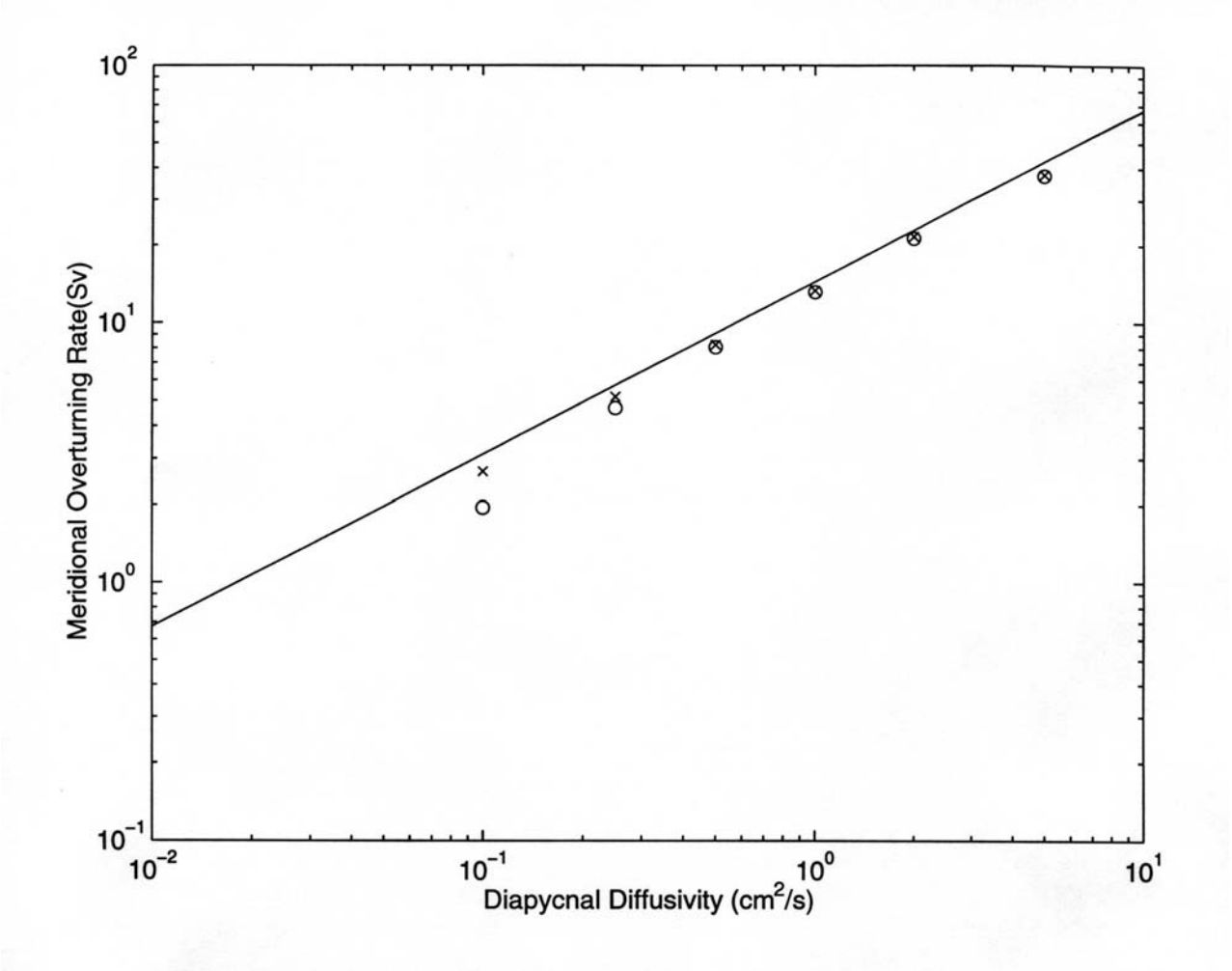

Figure 1. Comparison of the scaling results and numerical experiments under relaxation boundary conditions. The solid line represents the scaling theory, and the "x" and "o" represent numerical runs without and with wind stress respectively. Care was taken to avoid artificial diapycnal mixing due to lateral mixing acting on sloping isopycnals. (Zhang et al, 1999)

Thus, knowledge of the vertical diffusivity K is essential for understanding how the oceans transport and sequester heat. However, for many years there seemed to be too little mixing in the ocean to explain the observed meridional overturning rate. That is, an average $K = 1 \times 10^{-4}$ m^2/s is required, but observations of turbulence in the thermocline yielded a value that was an order of magnitude too small.

Intermittency of mixing.

Turbulence is relatively rare in the stratified ocean, occurring 1-5% of the time. It is also generally weak, and limited in vertical extent to a few meters. Shear instability of the internal wave velocities is the primary cause. Low frequency near- inertial waves, with a predominately horizontal velocity, are the most energetic contributors to mixing in the thermocline and upper ocean. Waves of tidal frequencies appear to be important in the deep ocean near topography.

Deep-ocean turbulence is measured with large, free-fall profilers which document the meter-scale density and velocity structure as well as the centimeter scale dissipation rates of thermal variance (χ) and turbulent kinetic energy (ε).

Measurement of oceanic microstructure:

Most often, the dissipation rates of turbulence and thermal variance are measured with a drop-sonde, either large and free-falling like the High Resolution Profiler (below), or small and tethered for upper ocean work. Typical instrument fall rates are ~ 0.5 m/s.

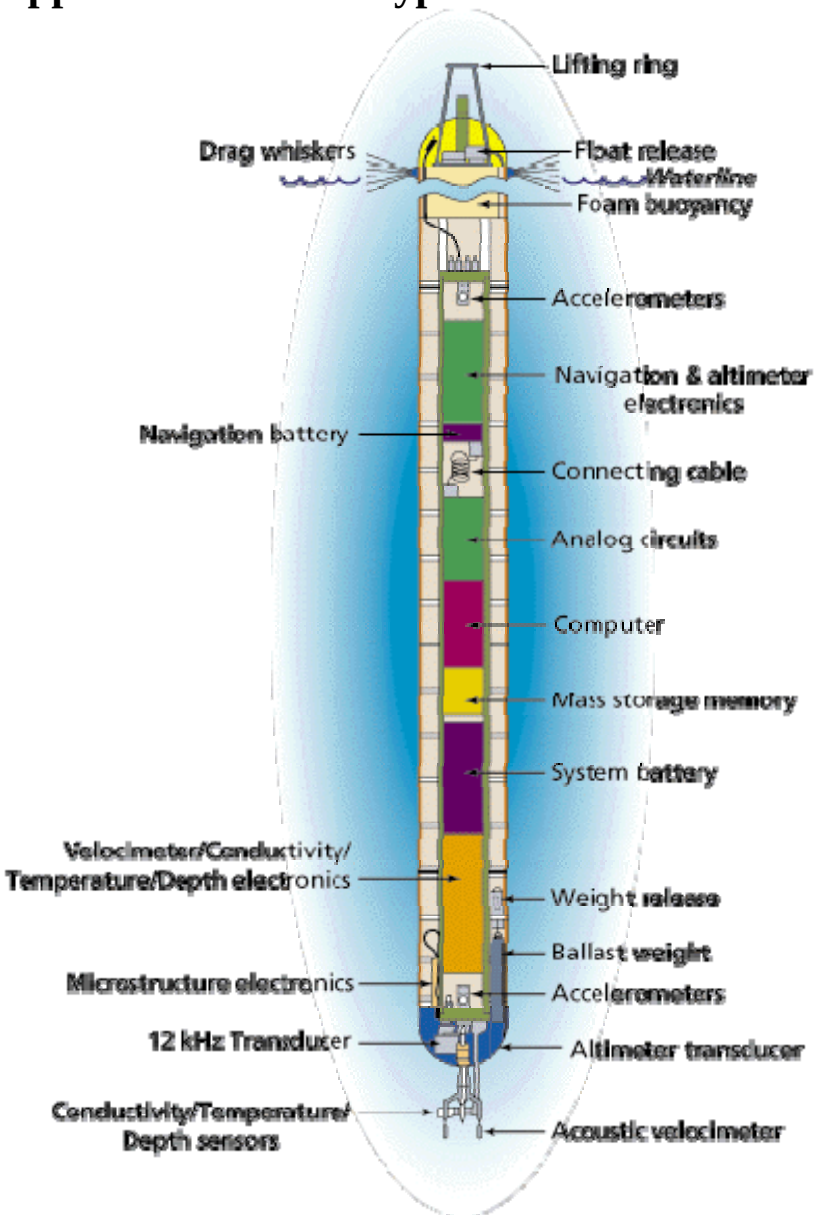

Figure 2. The High Resolution Profiler of Schmitt et al, 1988. This free-fall device drops weights at a pre-programmed depth or range above the bottom to return to the surface for retrieval and data download.

Temperature microstructure:

In order to estimate the dissipation rate of thermal variance (χ), it is necessary to measure the gradients of temperature to scales less than that of the Batchelor scale, ($L_B = 2\pi\left(\frac{\varepsilon}{\nu\kappa_\theta^2}\right)^{-1/4}$), which is generally a centimeter or less. With the fall rate at 0.5m/s, temporal resolutions to 30-50 Hz are required. Such fast response can only be achieved by very small sensors, such as thermocouples or thermistors. By far the most popular ocean micro-temperature sensor is the FP07 glass coated thermistor of Thermometrics.

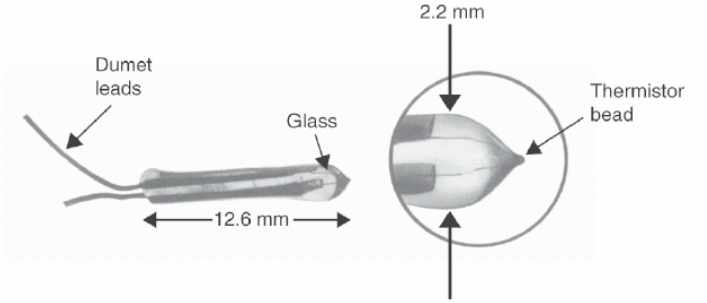

Figure 3, The FP07 by Thermometrics. The small thermistor bead is encapsulated in a fragile glass tip.

Thermistors have a large resistance change with temperature, and are much more sensitive than platinum resistance thermometers (PRTs) or thermocouples, though are not as stable as PRTs. This is fine for microstructure work, as there is generally a stable thermometer on the instrument for a running calibration. The FP07 is also prone to development of microcracks in the glass coating when subjected to the high pressures of the deep sea.

Since ocean temperature gradients are weak in the mixed layer and in the abyss, it is also necessary to "pre-emphasize" the electronic signal from the sensor, so that the output is proportional to the rate of change of temperature (and thus temperature gradient at constant fall rate). This gives a better signal to noise ratio for digitization.

Figure 4. Temperature and temperature gradient data from a dropsonde deployed in a Mediterranean salt lens (Oakey, 1988). The intermittency is typical. Hydrodynamic regimes change quickly in the stratified ocean, and much of the signal observed here may be due to double diffusion.

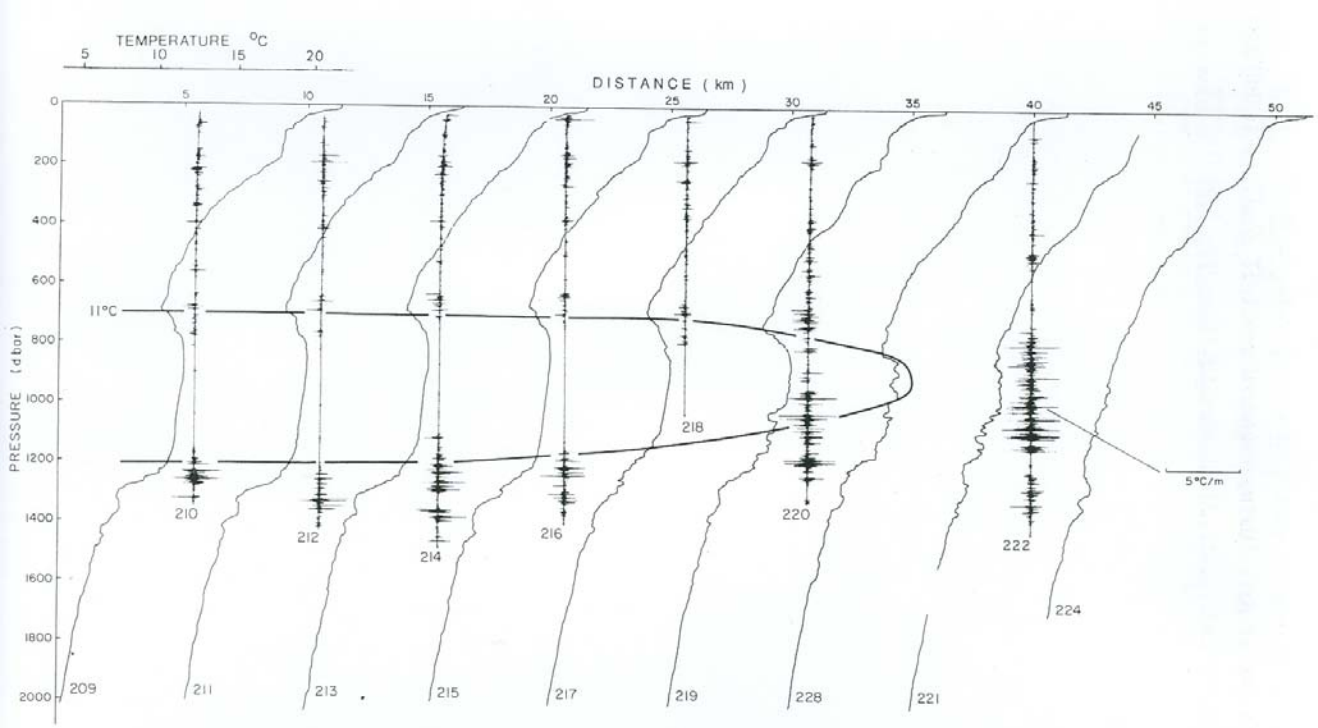

Fig. 1. The temperature structure (thin solid lines) and the corresponding temperature microstructure ('wiggly lines') is shown for a Mediterranean salt lens in the Canary Basin. The heavy 11 °C temperature contour marks the core of the MEDDY. Microstructure is most intense at the periphery.

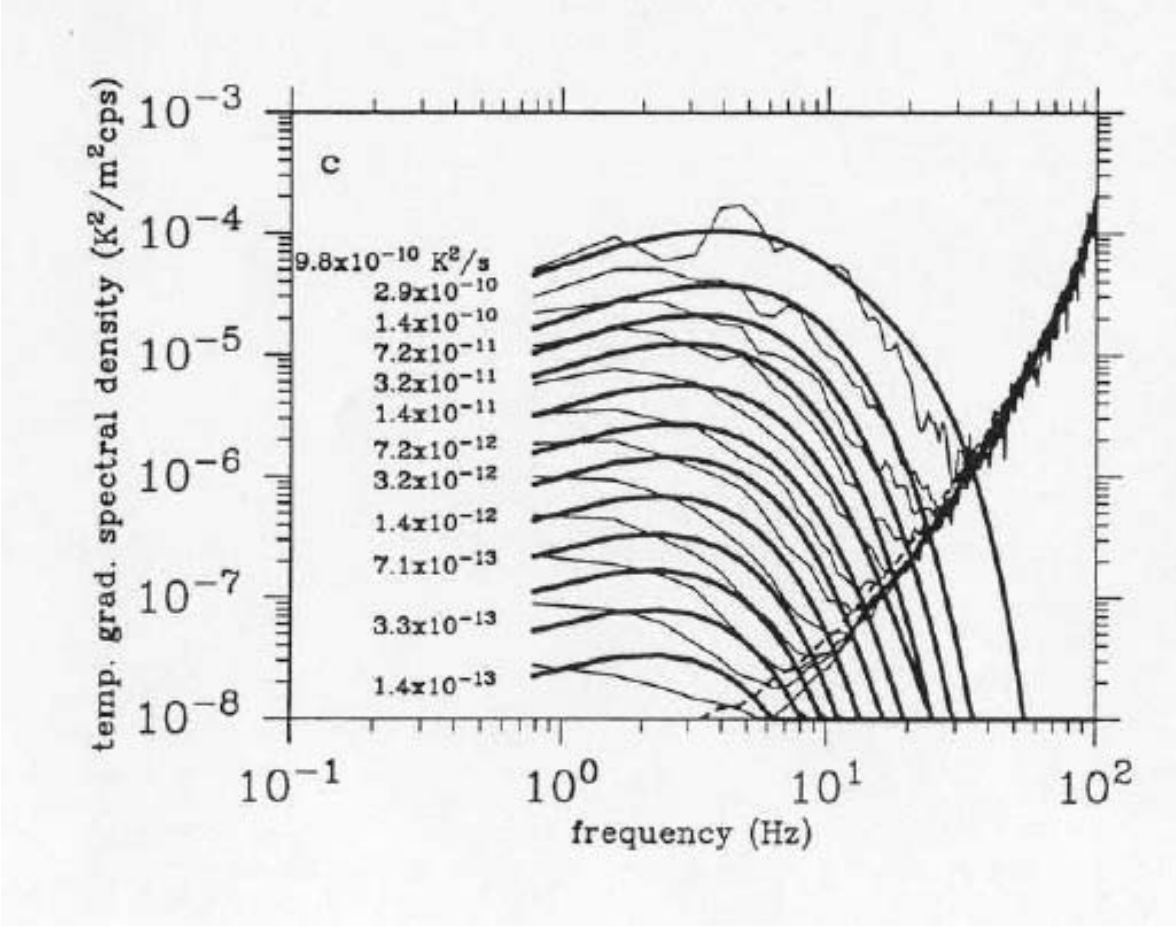

Figure 5. Spectra of the vertical temperature gradient from the High Resolution Profiler at different values of χ, with fits of the Batchelor spectrum shown as the smooth curves. The dashed line represents the noise level of the electronics.

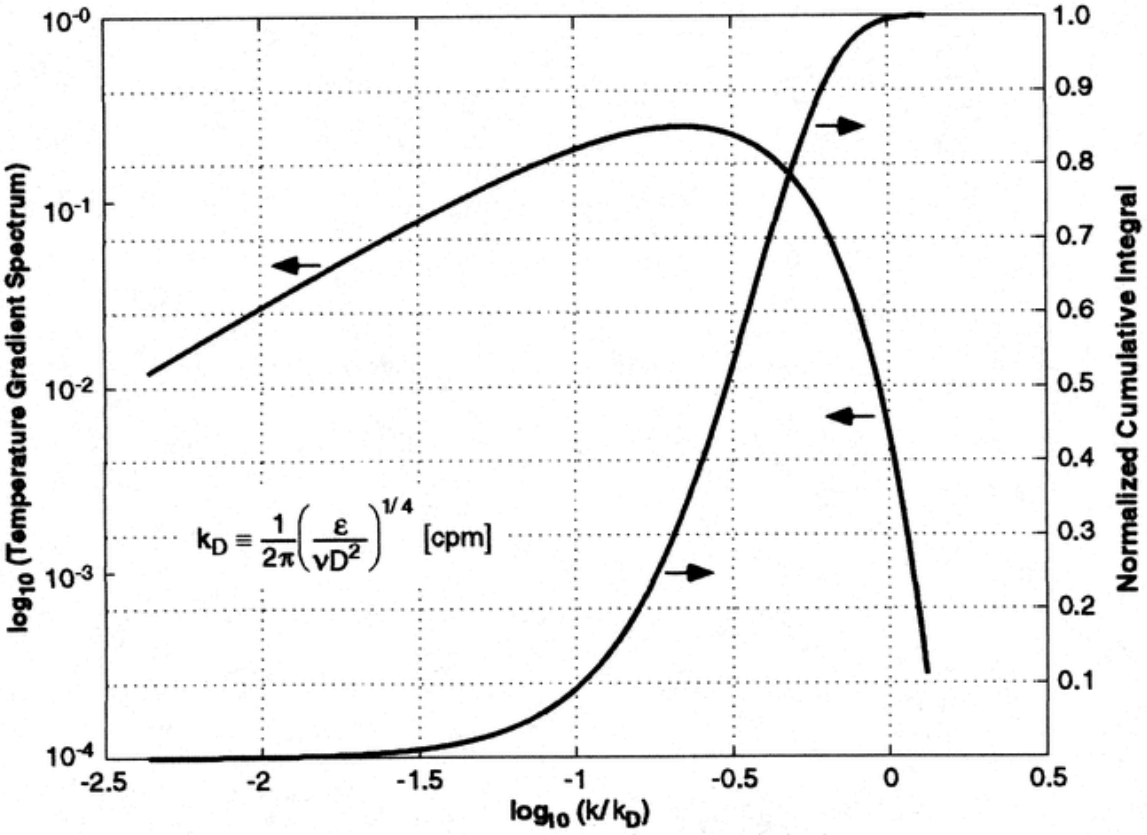

Figure 6. From Gregg (1999, *Journal of Atmospheric and Oceanic Technology:* Vol. 16, No. 11, pp. 1483–1490), showing one-dimensional temperature gradient spectrum, in arbitrary units, and its normalized cumulative integral. The spectrum is obtained by integrating the three-dimensional form derived by Batchelor (1959).

Use of temperature microstructure data.

From thermal variance equation, we assume a production – dissipation balance after Osborn & Cox (1972). That is, with

$$\theta \equiv \bar{\theta}(z) + \theta'(x, y, z, t)$$

Define the dissipation rate as:

$$\chi_\theta \equiv 2\kappa_\theta \iiint \left(\frac{\partial \theta'}{\partial x_i} \right)^2 dxdydz \cong 6\kappa_\theta \left\langle \theta_Z'^2 \right\rangle$$ **(isotropy)**

Then the "down gradient heat flux" is equal to ½ the dissipation rate:

$$\left\langle w'\theta' \right\rangle \frac{\partial \bar{\theta}}{\partial z} = \frac{\chi_\theta}{2}$$

This allows definition of an eddy diffusivity for heat:

$$\left\langle w'\theta' \right\rangle = K_\theta \frac{\partial \bar{\theta}}{\partial z}$$

$$K_\theta = \frac{\chi_\theta}{2\bar{\theta}_Z^2}$$

$$K_\theta = \frac{< \theta_Z'^2 >}{\bar{\theta}_Z^2} \kappa_\theta = C\kappa_\theta$$

Where *C* is the "Cox number".

Velocity microstructure:

In order to measure the small-scale shear in the ocean, very sensitive piezoelectric probes are used. These are designed to detect the sideways hydrodynamic lift forces acting on a small parabolic probe with a large translation velocity.

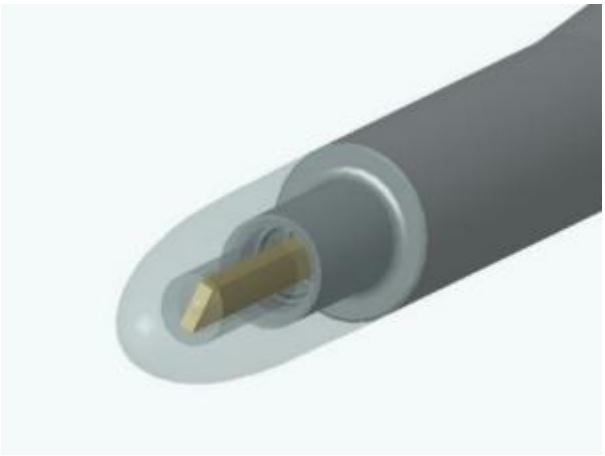

Figure 7. Piezoceramic beam (yellow), with one end anchored and the other encased in a flexible silicone rubber shroud. Electrodes on either side of the beam pick up changes in charge as the beam experiences sideways forces due to turbulence in the water. The sensitivity of the probe is dependent of the speed of the oncoming flow. Because of its symmetric shape, no side forces are experienced if the flow is free of turbulence. However, variations in the horizontal component of velocity change the angle of attack and generate lift that is readily detected by the sensitive piezoelectric beam.

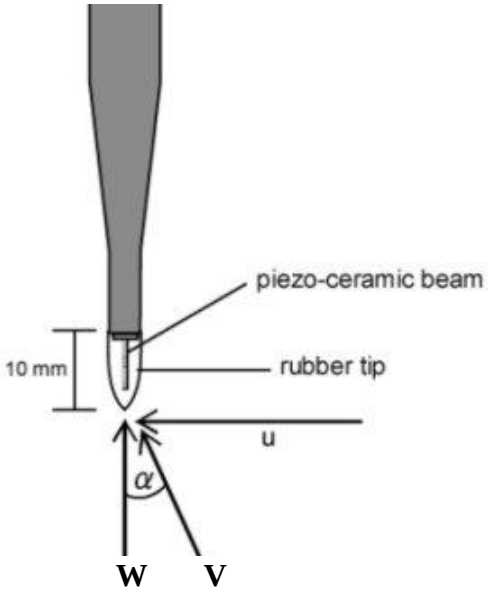

Figure 8. For a piezoceramic lift probe falling at large rate W, any small horizontal velocity (u) induces a slight change in the angle of attack on the tip of the probe, generating a lift force. Calibration involves measuring this lift force as a function of angle of attack in a known steady flow.

$$lift \sim \rho \frac{\bar{W}^2}{2} \sin\alpha$$

$$\sim \rho \frac{\bar{W}^2}{2} \frac{u(t)}{\bar{W}} \sim \frac{\rho}{2} \bar{W} u(t)$$

With a constant fall rate *W*, the output of the beam is amplified and differentiated to give a signal *E* proportional to the time rate of change of *u*, which, by Taylor's frozen field assumption, is proportional to the vertical shear, u_Z.

$$E(t) \approx \bar{W} u(t)$$

$$u(t) \approx \frac{E(t)}{\bar{W}}$$

$$\frac{\partial u}{\partial z} \approx \frac{\partial E}{\partial t} \frac{1}{W^2}, \qquad (with \quad \frac{\partial E}{\partial z} = \frac{1}{W} \frac{\partial E}{\partial t})$$

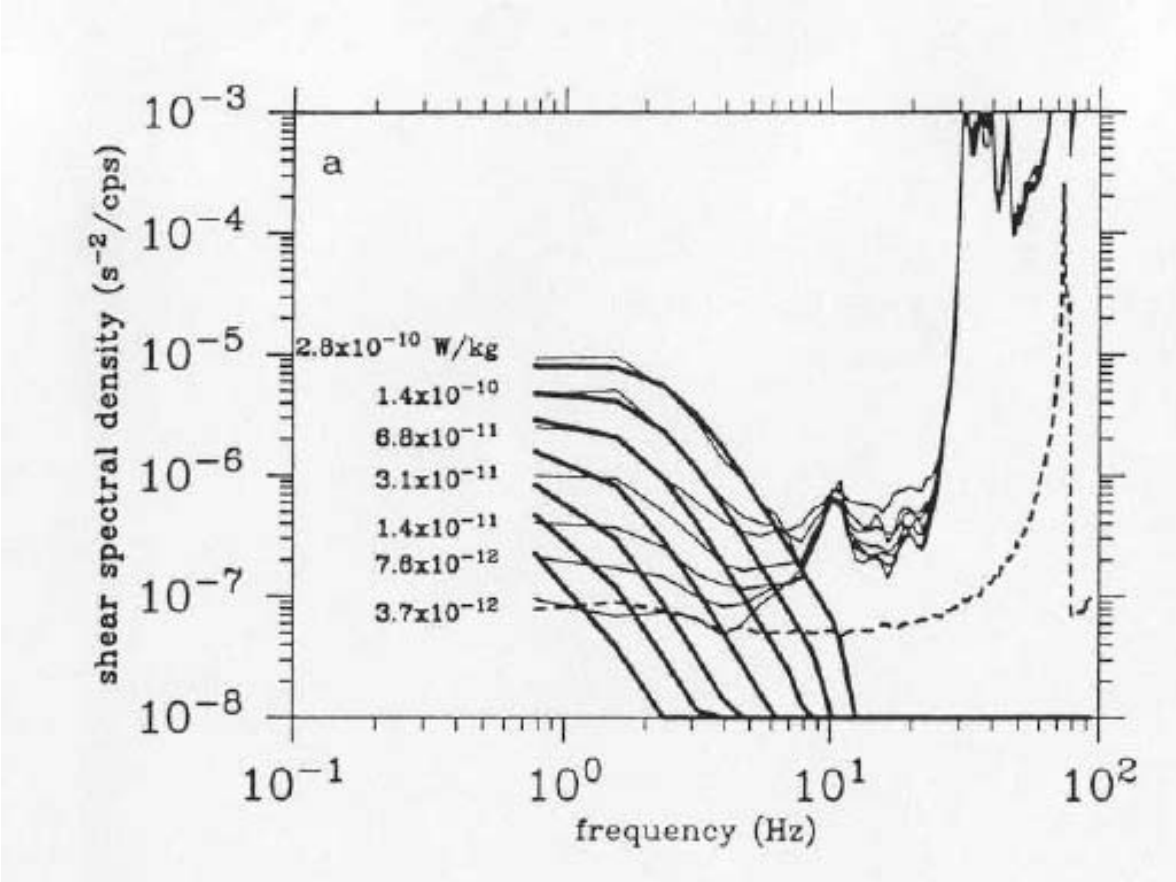

Figure 9. Spectra of vertical shear from a shear probe at different (low) dissipation levels. Dark solid lines are "Nasmyth" universal curves (Nasmyth, P. W., 1970: Oceanic turbulence. Ph.D. thesis, University of British Columbia, 69 pp) and the dashed line is the electronic noise of the amplifier. There are vibrational peaks at 10 Hz and above, so the variance in the spectra is integrated only out to the minimum in order to estimate ε.

Use of velocity microstructure: in the turbulent kinetic energy equation, assume production-dissipation balance as in Osborn (1980). For $U = \bar{U} + u'$ etc:

$$\left\langle u'w' \right\rangle \bar{U}_Z = \frac{g}{\rho} \left\langle \rho' w' \right\rangle - \varepsilon$$

We estimate ε using isotropy assumption and measurements of u'_Z :

$$\varepsilon = \frac{15}{2} \nu \left\langle u_z'^2 \right\rangle \qquad \textbf{(W/kg = m}^2\textbf{/s}^3\textbf{)}$$

Using the "flux" Richardson Number:

$$R_F \equiv \frac{g < \rho' w' >}{\rho < u'w' > \bar{U}_Z} \qquad \textbf{(~ 0.15 – 0.20)}$$

the buoyancy flux is related to the dissipation by:

$$\frac{g < \rho' w' >}{\rho} = \frac{R_F}{(1 - R_F)} \varepsilon = \Gamma \varepsilon$$

Define an eddy diffusivity by $< \rho' w' > = K_\rho \bar{\rho}_Z$, then:

$$K_\rho = \Gamma \frac{\varepsilon}{N^2}$$

If we compare K_θ and K_ρ we find they are equivalent when:

$$\Gamma = \frac{N^2 \chi}{2 \bar{\theta}_Z^2 \varepsilon} \approx 0.2$$

Oceanic data from non-double-diffusive stratifications generally agree with laboratory and numerical simulations that $\Gamma \approx 0.2$ for internal wave breaking in the stratified interior (Oakey, 1988). However, it can be much lower in strongly sheared and weakly stratified boundary layers.

Some observational results from microstructure and tracer release experiments:

1. **The main thermocline has generally weak turbulence, such that K_ρ is ~ 1 x 10^{-5} m^2/s.**

2. **The levels of turbulence can be related to the intensity of finescale (10m) shear due to internal waves.**

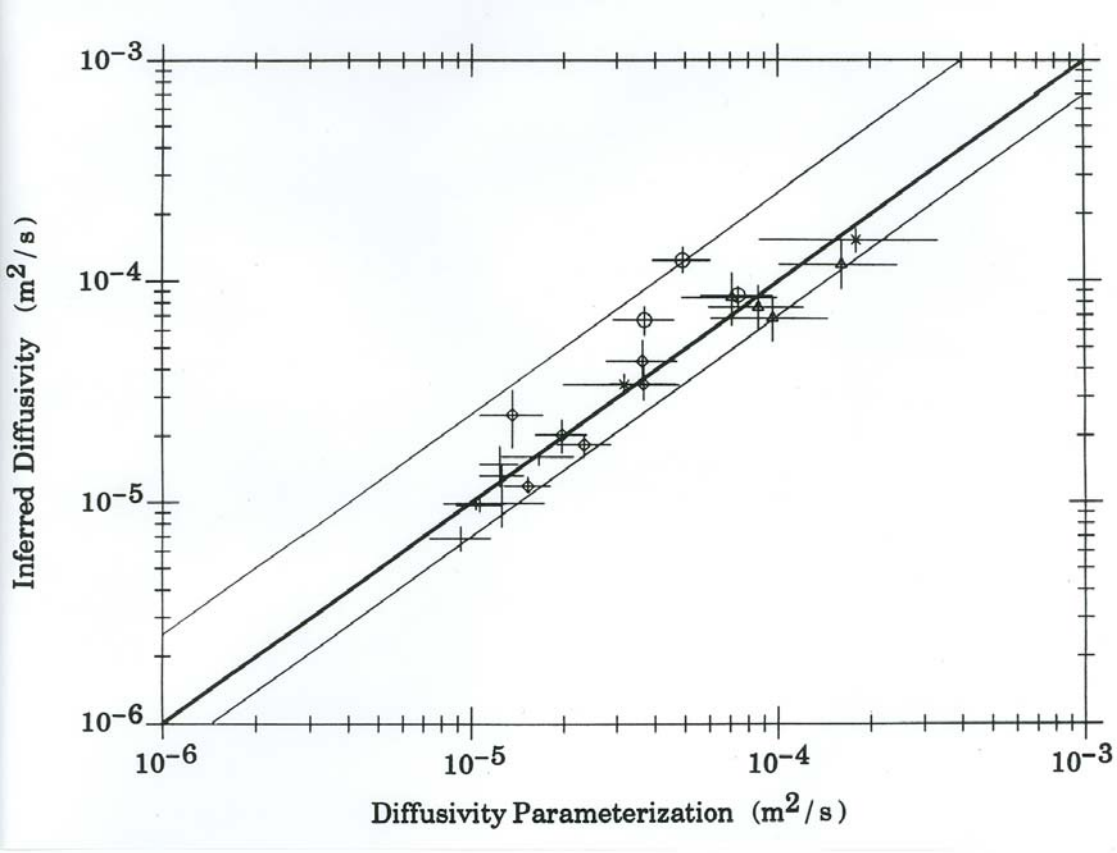

Figure 10. Plot of diffusivity estimated from measurements of ε compared against a parameterization based on internal waves shears at 10 m scales (From Polzin et al, 1995; see also Gregg, 1989).

3. **The abyss can have strong turbulence, if the bottom is "rough" and bottom velocities significant. Mechanism seems to be internal wave generation by the tides, and propagation into the stratified water above.**

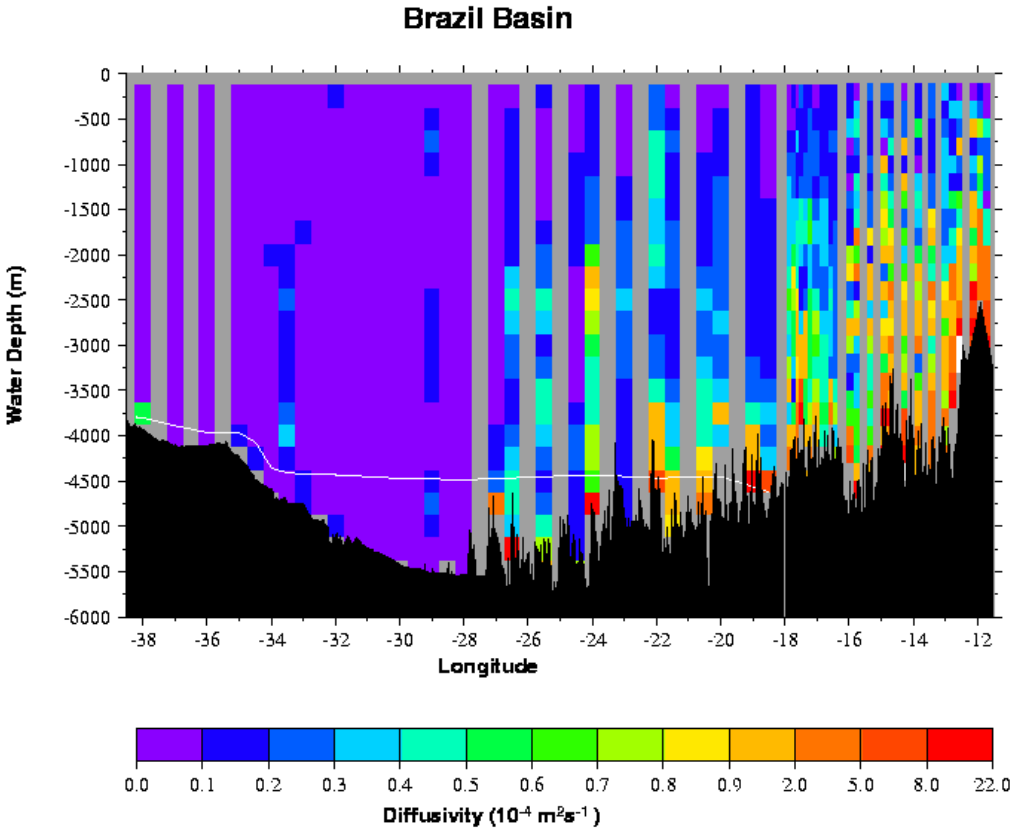

Figure 11. Composite section of diffusivity (based on observed ε and Osborn (1980) relation) across the Brazil Basin (Polzin et al, 1997). Turbulence is much enhanced over the irregular topography near the Mid Atlantic Ridge, and very weak over the abyssal plains to the west. A tracer release experiment has confirmed the high diffusivities near the ridge (Ledwell et al, 2000).

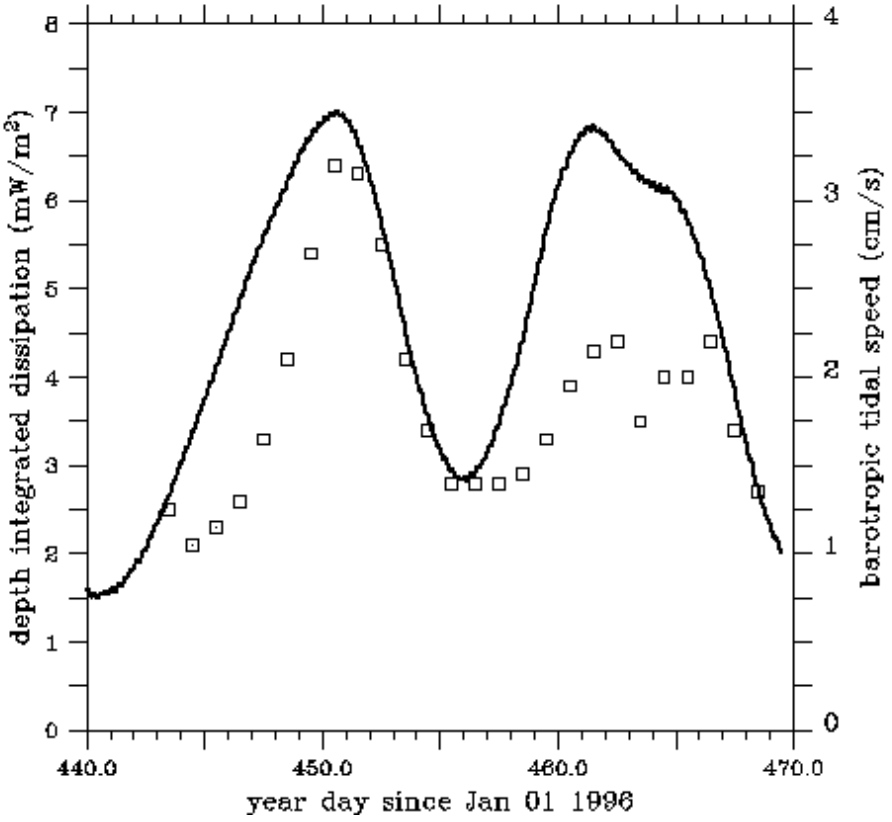

Figure 12. Vertically integrated dissipation rate compared with the estimated tidal speeds for the sampling period of a Brazil Basin cruise. Modulation with the strength of the fortnightly tide (beating of lunar and solar semidiurnal tides) is suggested.

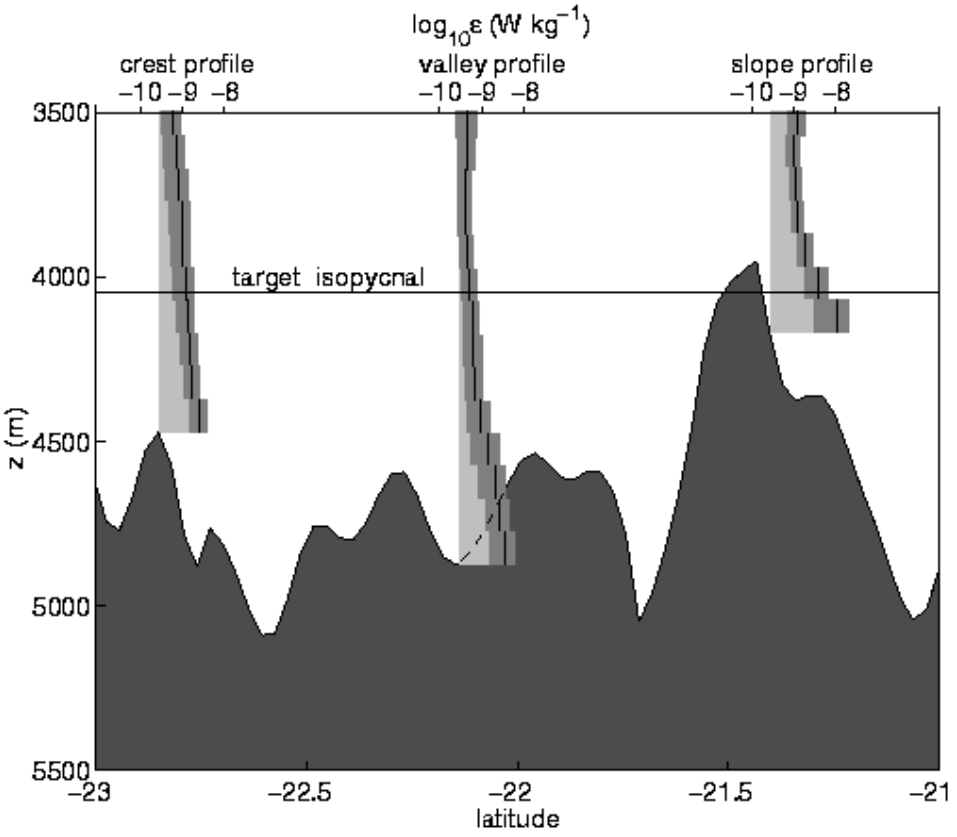

Figure 13. Average dissipation profiles with height above bottom for ridge crests (left), valleys (center), and slopes (right). Slopes showed the highest near bottom dissipations and the smallest decay with height. A passive tracer (SF_6) was released on an isopycnal with a mean depth just over 4000m.

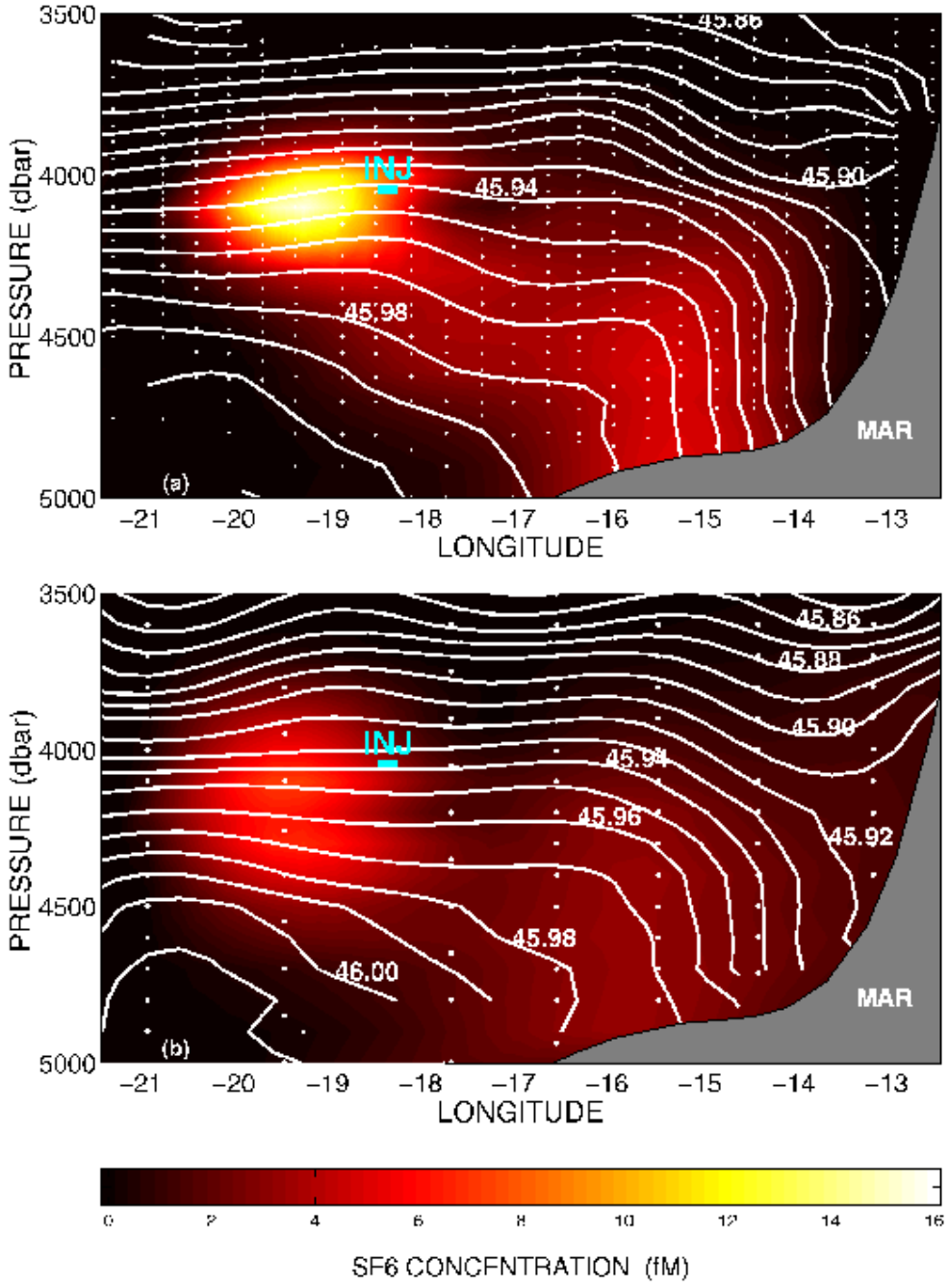

Figure 14. Tracer concentrations along a west to east canyon section approaching the mid-Atlantic Ridge on the right. Top: after 14 months. Bottom: after 26 months. Blue bar = injection site, white lines = isopycnals.

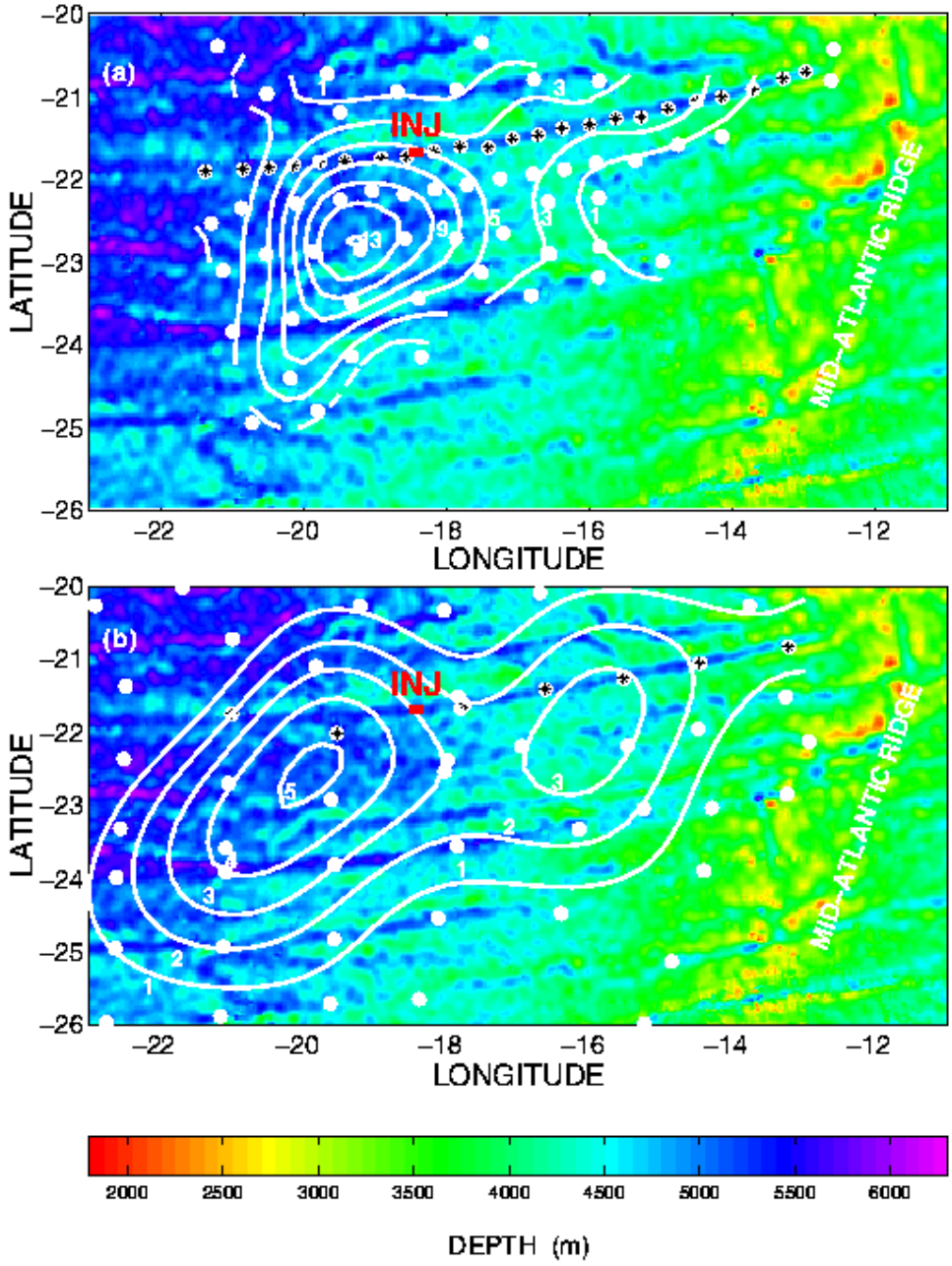

Figure 15. Tracer distribution at 14 months (top) and 26 months (bottom) after injection. The red bars labeled 'INJ' mark the release site of the tracer. The contours denote the column integral of SF_6 (in nmol/m^2) and colours denote bottom depth. The station positions are shown as white dots; those with stars are used for the sections in the fracture zone valley of Figure 13. Southerly latitude and westerly longitude are shown as negative numbers.

4. Spatially variable mixing rates have consequences for the interior baroclinic circulation of the ocean.

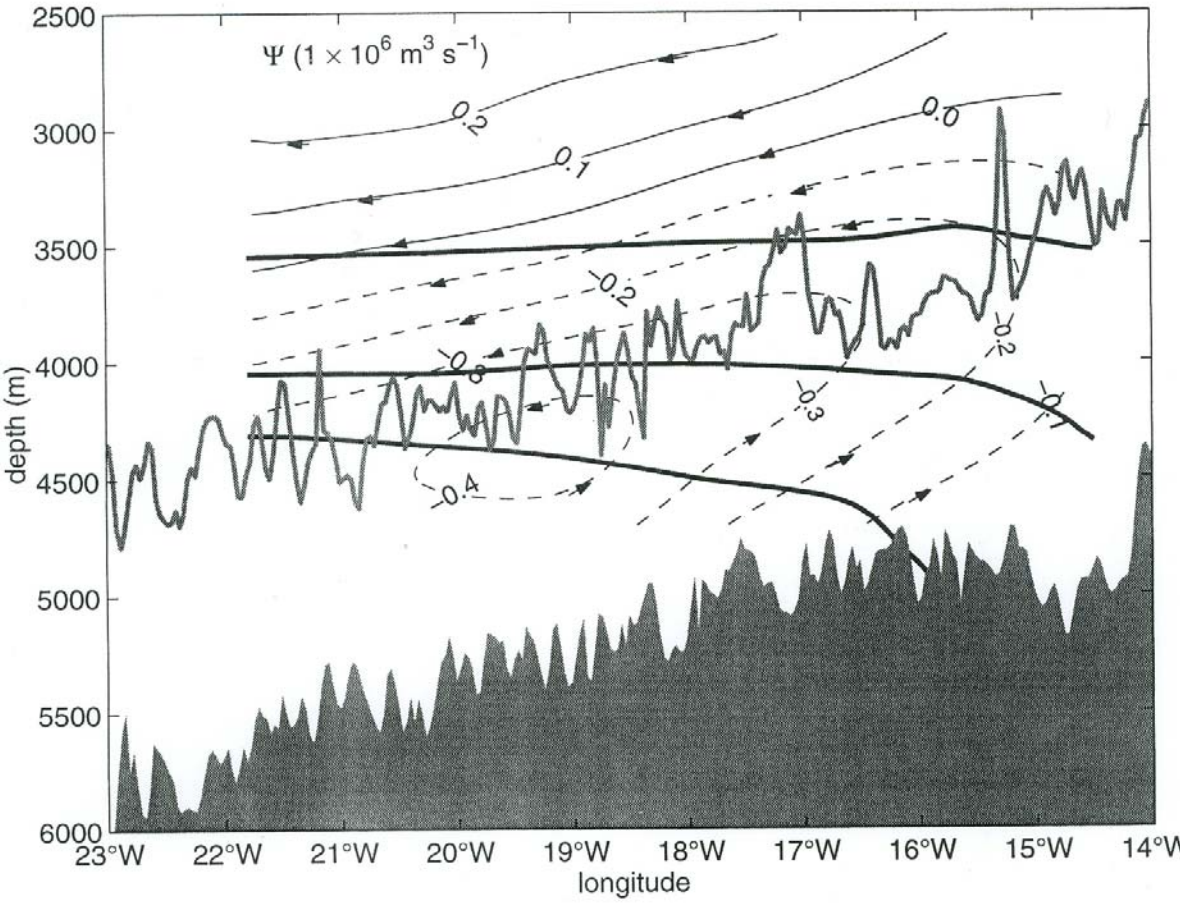

Figure 16. The interior circulation streamfunction suggested by the variation of turbulent mixing rate near the Mid-Atlantic Ridge. This represents the circulation over a latitude band in which the deepest canyon depths are represented by the black bottom, and the shallowest peaks represented by the grey line. The increase of mixing rate approaching the ridge requires up-canyon flows across the density lines shown. (St Laurent et al, 2001).

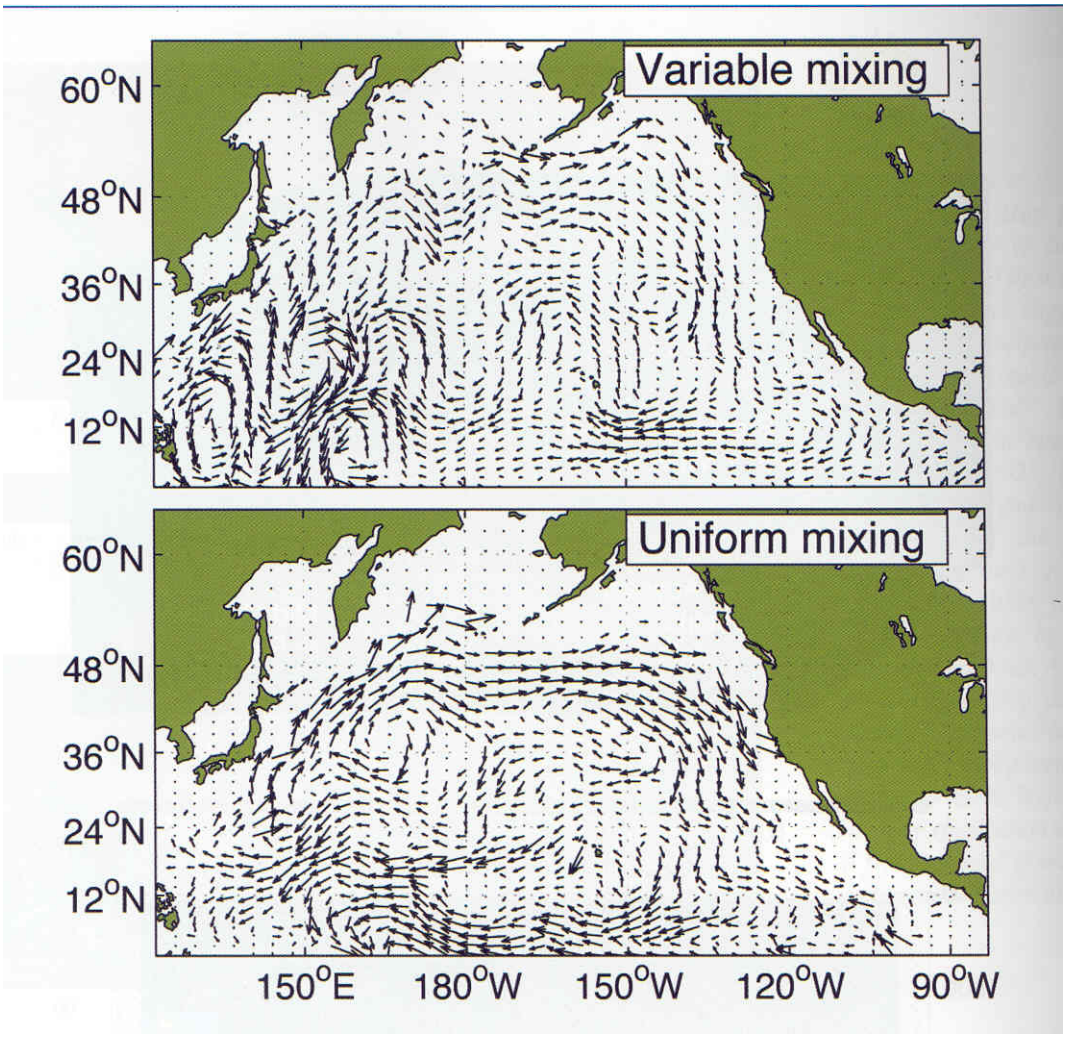

Figure 17. Deep circulation in a model with spatially variable mixing (top figure) compared with uniform mixing (bottom). The variable mixing was prescribed by a model of internal wave generation by topography. (Simmons et al, 2004).

Osmidov and Thorpe scales:

The presence of turbulence in a stratified fluid allows the definition of another length scale. The Osmidov length is formed from ε and N, the buoyancy frequency of internal waves:

$$L_O \equiv \frac{\varepsilon^{1/2}}{N^{3/2}}$$

Typically, this is a meter or less in the weak turbulence of the thermocline, but can be tens of meters in near-bottom boundary layers.

A related length is the Thorpe scale, L_T , which is defined in gravitationally unstable density profiles as the RMS displacement required to re-stratify the overturned fluid. A sorting algorithm is used to reorder the profile to a stable configuration. Ocean turbulence data indicate that:

$$L_O \simeq (0.8 - 0.95) L_T$$

The Thorpe scale can be easily estimated from high quality density profiles, in contrast to turbulence profilers, so makes possible reasonable inferences about mixing in a wide array of data sets.

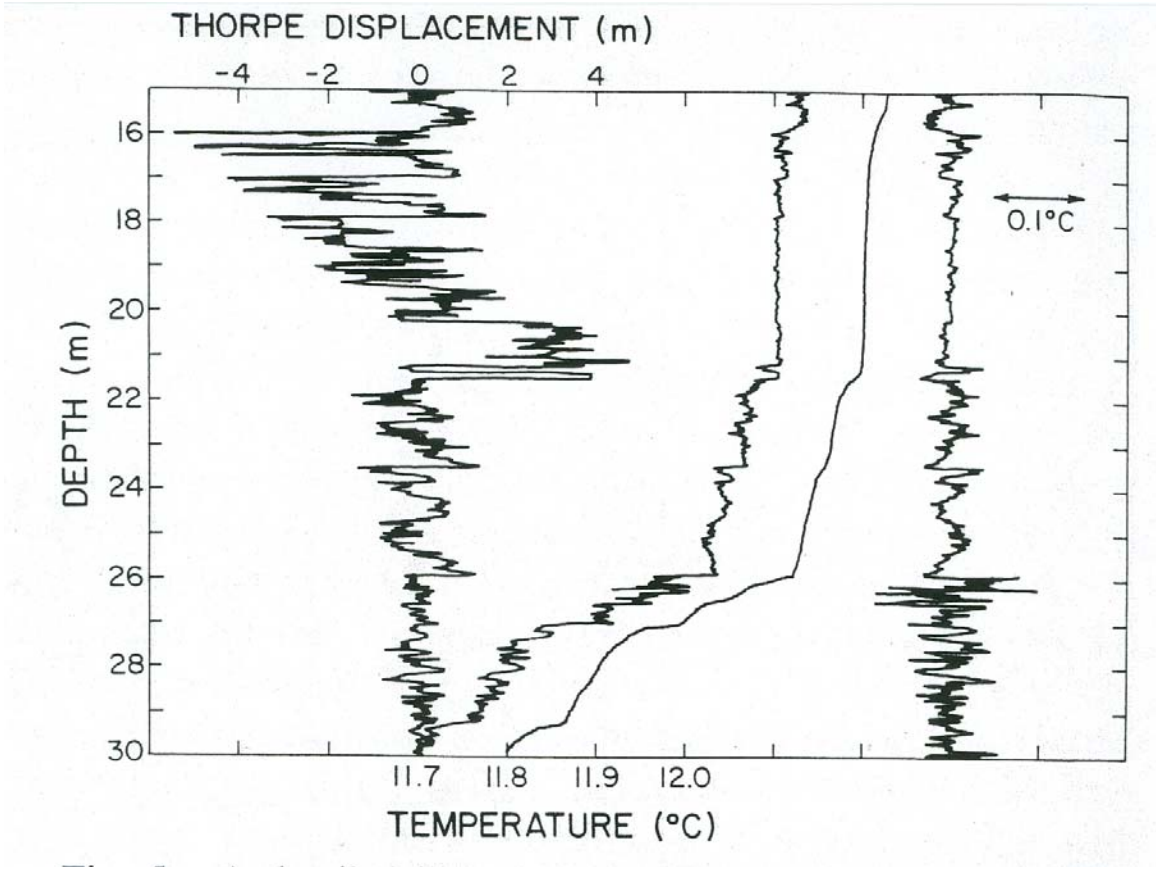

Figure 18. A detailed illustration of Thorpe displacements. From left to right: displacements, observed temperature, ordered temperature, and temperature fluctuations (difference between ordered and unordered temperature)

Reference:

Dillon, T. M., 1982. Vertical overturns: a comparison of Thorpe and Ozmidov Length Scales. J. Geophys. Res., 87, 1847-1854.

For parameterizations of mixing see also:

Ferron, B., H. Mercier, K. Speer, A. Gargett and K. L. Polzin. 1998. Mixing in the Romanche Fracture Zone. J. Phys. Oceanog. 28, (10), 1929-1945.

References:

Batchelor, G. K., 1959: Small-scale variation of convected quantitites like temperature in turbulent fluid. *J. Fluid Mech.,* 5, 113–139.

Gregg, 1999. Uncertainties and Limitations in Measuring ϵ and χ_T *Journal of Atmospheric and Oceanic Technology:* Vol. 16, No. 11,pp. 1483–1490.

Gregg, 1989. Scaling turbulent dissipation in the thermocline. J. Geophys. Res. 94, 9686-9698.

Huang, R. X., 1999. Mixing and Energetics of the Oceanic Thermohaline Circulation. Journal of Physical Oceanography, 29, (4), 727-746.

Ledwell, J. L., E. T. Montgomery, K. L. Polzin, L. C. St. Laurent, R. W. Schmitt and J. M. Toole, 2000. Evidence for enhanced mixing over rough topography in the abyssal ocean. *Nature*, 403(6766), 179–182.

Munk, W. H., 1966. Abyssal Recipes. Deep Sea Research,13 707-730.

Munk, W. H., and C. Wunsch, 1998. Abyssal Recipes II: Energetics of tidal and wind mixing

Nasmyth, P. W., 1970: Oceanic turbulence. Ph.D. thesis, University of British Columbia, 69 pp.

Oakey, N., 1988. Estimates of mixing inferred from temperature and velocity microstructure. . In: *Small-Scale Turbulence and Mixing in the Ocean*, J.C.J. Nihoul and B. M. Jamart (Editors), Elsevier Science Publishers, Amsterdam, 239-247.

Osborn, T. 1980. Estimates of the local rate of vertical diffusion from dissipation measurements. J. Phys. Oceanogr., 10, 83-89.

Osborn, T and C. Cox, 1972. Oceanic Finestructure, Geophys. Fluid Dynamics, 3, 321-345.

Polzin, Kurt L., John M. Toole and Raymond W. Schmitt, 1995. Finescale parameterizations of turbulent dissipation. *Journal of Physical Oceanography*, 25, 306–328.

Polzin, K. L., J. M. Toole, J. R. Ledwell and R. W. Schmitt, 1997. Spatial variability of turbulent mixing in the abyssal ocean. *Science*, 276, 93–96.

St. Laurent, Louis C., John M. Toole, and Raymond W. Schmitt, 2001. Buoyancy forcing by tur-bulence above rough topography in the abyssal Brazil Basin. *Journal of Physical Oceanog-raphy*, 31, 3476–3495.

Schmitt, Raymond W., John M. Toole, Richard L. Koehler, Edward C. Mellinger and Kenneth W. Doherty, 1988. The development of a fine- and microstructure profiler. *Journal of Atmospheric and Oceanic Technology*, 5(4), 484–500.

Simmons, H. L., S. R. Jayne, L. St. Laurent and A. Weaver, 2004. Tidally driven mixing in a numerical model of the ocean general circulation. Ocean Modelling, 6, 245-263.

Stern, M. E., 1975. Ocean Circulation Physics. (Chap. 12: Horizontal Convection and Thermoclines). Academic Press, New York. 246pp.

Zhang, J., R. W. Schmitt, and R. X. Huang, 1999. The Relative Influence of Diapycnal Mixing and Hydrologic Forcing on the Stability of the Thermohaline Circulation. Journal of Physical Oceanography, 29, (6), 1096-1108.